

Synergy Effects in Blended Electrodes for Li-ion Batteries: A Conceptual Clarification

Christian Heubner,^[a] Tobias Liebmann,^[b] Christoph Lämmel,^[a] Michael Schneider,^[a] and Alexander Michaelis^[a, b]

The use of electrodes with multiple active materials is considered a promising approach to develop advanced Li-ion batteries. Recent studies even point to synergistic effects in terms of rate performance. However, the origin of synergistic effects is still insufficiently understood to enable targeted material and design development and to optimize batteries accordingly. Using straightforward equivalent circuit modeling combined with electrochemical studies, we reveal that improvements in rate capability are an intrinsic property of blended electrodes. The electrical parallel connection of the components in the composite electrode allows the applied current to be distributed among the components in a way that the voltage

losses become minimal. This way, rate-limiting components can still contribute to the electrode's capacity at high loads, which makes blended electrodes particularly attractive, e.g., for applications that must be able to handle high pulse loads. Based on the results, rational design principles are derived by means of a systematic sensitivity analysis, quantifying the influence of the individual active material properties. These findings greatly contribute to the understanding of the internal dynamics and synergy effects in blended electrodes and support the targeted development of advantageous material combinations and electrode designs for future Li-ion batteries.

1. Introduction

Increasing energy and power density is one of the most important goals of battery research and development in order to meet demanding applications such as electric mobility or renewable energy storage.^[1–4] Besides improvements regarding cell concepts and electrode architectures, the development of advanced active materials is considered the most promising approach to optimize the performance of Li-ion batteries (LIB).^[5,6] Common cathodes for LIB are based on an active material (AM), which is either a phospho-olivine, layered oxide or spinel type. Each class of AM has individual advantages and disadvantages. For example, phospho-olivines, such as LiFePO₄, exhibit high thermal and chemical stability, but have a relatively low voltage and thus energy density. Layered oxides, such as LiNi_xCo_yMn_zO₂, have high energy density but suffer from thermal instability and moisture sensitivity. Spinel-type materials, such as LiMn₂O₄, exhibit high rate capability and low cost, but have relatively low energy density and poor chemical

stability against liquid electrolytes.^[7] Mixing different AMs in one electrode is considered a promising approach to combine their individual advantages and compensate detrimental properties.^[8–11] While the very purpose of blending AMs is to compensate for their individual drawbacks, synergistic effects have recently been reported, where the performance of the blended electrodes exceeds expectations based on the weighted superposition of the components' properties. Although blended cathodes are already used in modern electric vehicles based on positive empirical experience, the origin of synergistic effects is still quite poorly understood. This circumstance complicates the identification of advantageous compositions and designs. Synergies regarding cycle life performance^[12,13] and thermal stability^[14–16] of blended cathodes are reported by several groups. Furthermore, improvements in rate capability or average voltage have been repeatedly demonstrated for liquid^[15,17–22] and solid^[23,24] electrolyte systems. Since there are several definitions of "synergy", the choice of definition strongly influences the conclusion whether a measurement result indicates "synergy" or not.^[25] a) Synergy could be generally understood as a positive effect in the interaction of the individual components; b) Synergy could mean that the properties of the mixture exceed expectations based on the properties of the components in a positive sense. The term "disergy" is not very common, but has come to describe the opposite of synergy, i.e., that the properties of a mixture fall short of expectations. In the context of blended electrodes for LIB, the classification as 'synergistic' is commonly based on a comparison of the blend's properties with the weighted averaging of the behavior of the individual components. If the rate capability or the average voltage of the blended electrodes

[a] Dr. C. Heubner, Dr. C. Lämmel, Dr. M. Schneider, Prof. A. Michaelis
Mobile Energy Storage and Electrochemistry
Fraunhofer Institute for Ceramic Technologies and Systems IKTS
Winterbergstr. 28, 01277 Dresden, Germany
E-mail: christian.heubner@ikts.fraunhofer.de

[b] T. Liebmann, Prof. A. Michaelis
Institute of Materials Science
TU Dresden
Helmholtzstr. 7a, 01069 Dresden, Germany

 Supporting information for this article is available on the WWW under
<https://doi.org/10.1002/batt.202100171>

 © 2021 The Authors. *Batteries & Supercaps* published by Wiley-VCH GmbH.
This is an open access article under the terms of the Creative Commons Attribution License, which permits use, distribution and reproduction in any medium, provided the original work is properly cited.

exceeds the theoretical predictions, synergistic effects are attested, corresponding to the definition b).

For example, synergistic effects were reported for blended cathodes including $\text{LiFe}_{0.3}\text{Mn}_{0.7}\text{PO}_4$ (LFMP), where the experimental results exceed the predicted capacity or average voltage at medium to high discharge rates.^[20–22] The prediction of the blends' properties was made by weighted superposition of the differential capacity profiles of the pure components obtained individually at different C-rates. The superiority of the experimental over the theoretical results was interpreted as reduced polarization, resulting from Li redistribution between the materials. Indeed, a redistribution of Li between the components of blended electrodes during cell relaxation has been observed in both experimental and theoretical studies.^[21,26,27] However, the significance of this effect under load has not yet been clarified. Comparable synergistic effects were found regarding the rate capability of $\text{LiNi}_{1/3}\text{Co}_{1/3}\text{Mn}_{1/3}\text{O}_2$ - LiMn_2O_4 blended electrodes.^[28] The expected capacity of the blended electrode for a given C-rate is estimated from the weighted superposition of component capacities measured independently at the same current density. The authors attribute the synergistic effect to increased diffusivity of Li-ions between particles, which reportedly reduces particle impedance and promotes rate performance. Our group has recently shown that basic electrochemical properties of blended electrodes, such as equilibrium voltage and entropy profiles, charge transfer resistance, and solid-state diffusivity, are consistent with theoretical predictions based on the components' properties.^[29] Accordingly, these properties cannot account for any synergistic effects in terms of average voltage and rate capability.

In the present study, the rate capability and average voltage of blended electrodes is investigated by means of electrochemical characterization and straightforward equivalent circuit modeling. The emergence of synergistic effects is demonstrated using an example blend system - LiMn_2O_4 (LMO) mixed with LiFePO_4 (LFP). By means of simplified equivalent circuit modeling, the influence of the parallel connection of the components in the mixture is demonstrated in comparison to the usual weighted superposition procedure. To estimate the

impact of the components' properties on the magnitude of synergistic effects, a sensitivity analysis is performed. The results shed light on the hitherto poorly understood synergistic effects in blended electrodes and refute several hypotheses from the literature. Implications of these findings for the predictability of the electrochemical properties of blended electrodes and the derivation of promising research and development approaches are briefly discussed.

2. Results and Discussion

2.1. Synergy Effects in the $\text{LiMn}_2\text{O}_4/\text{LiFePO}_4$ System

To exemplarily demonstrate the occurrence of synergistic effects, single component and blended electrodes with LiMn_2O_4 (LMO) and LiFePO_4 (LFP) as the active materials were prepared and investigated regarding their electrochemical performance. Figure 1 shows voltage profiles of single component LMO and LFP electrodes obtained at different C-rates. While the LMO electrode shows lower capacity at low discharge currents, it outperforms the LFP electrode in terms of rate capability. The attainable capacity of the LFP electrodes drops to zero for C-rates $> 1.0 \text{ C}$ (Figure 1b). In contrast, approximately 77% of the nominal capacity is obtained for the LMO electrode at 5.0 C (Figure 1a).

The voltage profiles obtained from the single component LMO and LFP electrodes were used to predict the properties of blended electrodes of different mass ratios. To estimate the voltage profile of a blended electrode at a given C-rate, researchers typically proceed as depicted in Figure 2: i) Voltage profiles of single component electrodes are measured at different C-rates. ii) The differential capacity of the single component electrodes is determined by numerical derivation of specific capacity over voltage obtained at the desired C-rate. iii) The differential capacities of the individual components are then superimposed, weighted according to the mass fraction in the blend, to determine the differential capacity of the blended electrode. iv) The obtained differential capacity of the blended electrode is numerically integrated over a certain voltage range

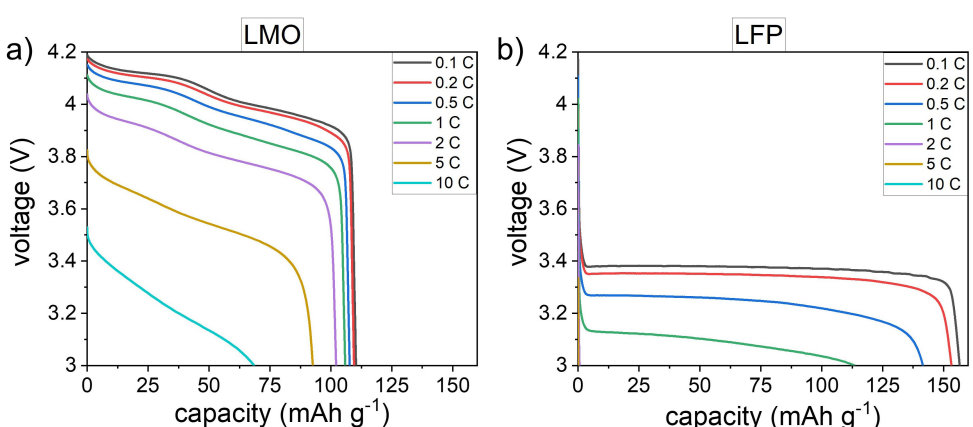


Figure 1. Voltage profiles of single component a) LMO and b) LFP electrodes at different C-rates.

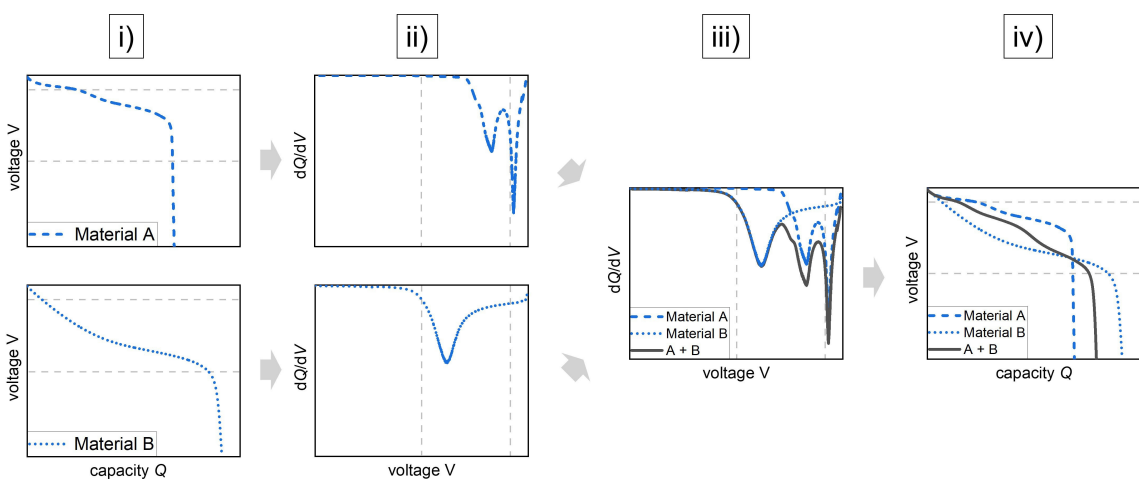


Figure 2. Schematic illustration of the weighted superposition procedure (WSP) used to estimate the voltage profile and corresponding specific capacity of blended electrodes. i) Voltage profiles and ii) differential capacity of the single component electrodes consisting of materials A and B. iii) weighted superposition of differential capacities and iv) voltage profile of the blended electrode obtained from numerical integration over a certain voltage range.

to determine the voltage profile and the corresponding specific capacity. This procedure will be referred to as the weighted superposition procedure (WSP) in the following.

Figure 3(a and b) shows voltage profiles of LMO/LFP blends at different C-rates measured experimentally and predicted theoretically by means of WSP for different mass ratios. At low C-rate (0.1 C), WSP predictions and experimental voltage profiles agree well with each other for both mass ratios, LMO:LFP 1:1 wt% (Figure 3a) and LMO:LFP 2:1 wt% (Figure 3b). For C-rates > 1.0 C, the experimental voltage profiles and WSP predictions start deviating from each other. Experimental results and WSP predictions were evaluated regarding specific capacity and average voltage (Figure 3c-f). For low C-rates, the experimentally achieved capacity and WSP predictions agree well (Figure 3c,d). At medium C-rates, the experimentally achieved capacity exceeds the WSP predictions. This behavior is usually attributed to synergistic effects related to the blending of different active materials.^[15,17–24] At high C-rates (> 5 C), the WSP predictions start to overestimate the experimental results, which might be considered as disergy effect. The magnitude of synergistic effects and the corresponding range of C-rates is larger for LMO:LFP 1:1 wt% compared to LMO:LFP 2:1 wt%. The behavior observed for the differences between experimentally achieved capacity and WSP predictions is also found for the average voltage (Figure 3e,f). At low C-rates, the experimentally obtained average voltage is consistent with the WSP predictions. For medium C-rates, WSP predictions underestimate the average voltage, which might indicate synergistic effects.^[15,17–24] At high C-rates, the experimental results are lower compared to the WSP predictions. Again, the magnitude and C-rate range of synergy slightly varies with the mass ratio of the components in the blend.

2.2. Equivalent Circuit Modeling

To investigate the origin of the differences between WSP predictions and experimental results, straightforward theoretical investigations were performed using equivalent circuit modeling (ECM). The ECM of electrochemical systems is well established for understanding and describing the effect of adsorption, reaction, and diffusion processes on the electric potential response as it represents electrode kinetics in a simple but sufficiently accurate manner.^[30,31] Note that the ECM performed here is not intended to simulate the experimental behavior of the LMO:LFP blend system, but is a simplified model for general understanding of specific aspects of blended electrodes. In blended electrodes for LIB, multiple types of AMs exist next to each other embedded in a porous carbon-binder matrix as schematically depicted in Figure 4(a). The electrochemical behavior can be described by a combination of different mechanism shown in the equivalent circuit in Figure 4(a). The Li-ion transport through the electrolyte and the electron conduction in the composite are described by a series of ohmic resistors, R_{el} and R_{ion} . The contact resistance between the porous composite and the current collector is modeled by an RC-element, representing the interfacial resistance, R_{cont} , and the corresponding capacitance, C_{cont} . The charge transfer reaction at the different active materials surfaces is described by RC-elements including the charge transfer resistance, R_{ct} , and the electrochemical double layer capacitance, C_{dl} . Solid-state diffusion in the different active materials is represented by a Warburg element, W_D . The Li-ion storage in the active material is modeled by the capacitance, C_{AM} .

For the sake of clarity, we simplify the equivalent circuit in Figure 4(a) to the basic properties that describe the electrochemical behavior of a blended Li-intercalation electrode in the time domain relevant for battery operation. The simplified equivalent circuit consists of a parallel connection of two serial R-C elements (cf. Figure 4b), each representing one of the blend's components. The resistors represent the sum of the

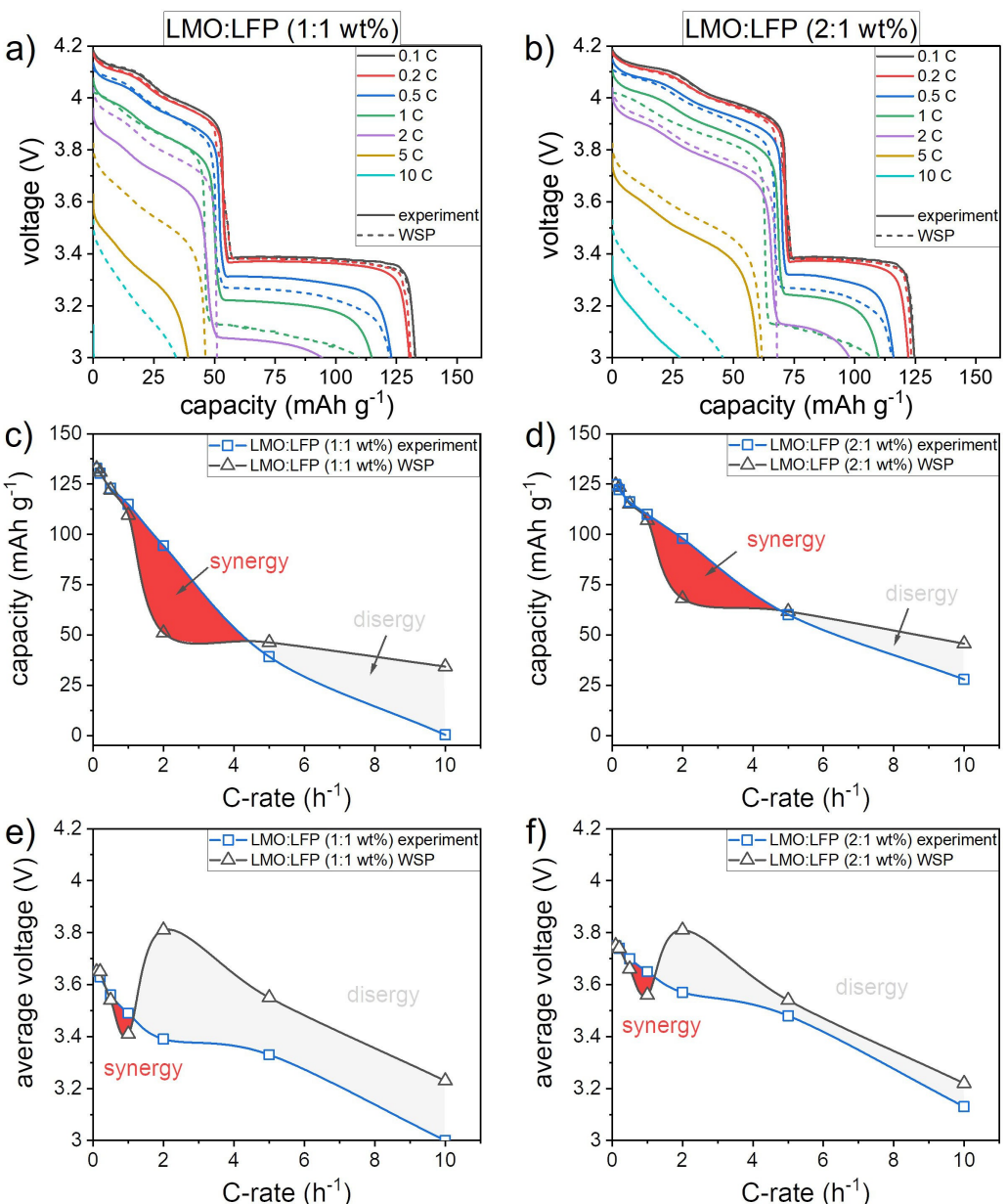


Figure 3. Voltage profiles of LMO/LFP blends at different C-rates measured experimentally and predicted based on the weighted superposition (WSP) of the components' properties for different mass ratios of LMO:LFP a) 1:1 wt% and b) 2:1 wt%. Specific capacity c,d) and average voltage e,f) obtained experimentally and predicted by WSP as a function of the C-rate. Regions in which synergy and disergy effects occur are indicated by the colored areas.

individual resistors ($R_{\text{el}}, R_{\text{ion}}, R_{\text{ct}}, R_{\text{cont}}, R_{\text{diff}}$) which limit the Li insertion into the components A and B. The corresponding capacitances describe the differential capacities of A and B. The charging of the electrochemical double layer is typically completed after a few seconds and can thus be neglected for typical durations of battery operation.^[32] The differential capacity of the active materials typically varies with equilibrium potential and the SOC, respectively. For the clarity of explanation, we use a constant differential capacity here. The simplified equivalent circuit to model the electrochemical behavior of single component electrodes is shown in Figure 4(c). Details on the following ECM are provided along with

the results, in the Materials and Methods Section and as Supporting Information (SI).

Figure 5 shows voltage profiles of single component electrodes at the 0.1 C (Figure 5a) and 6 C (Figure 5a) discharge rate obtained from ECM for typical properties of battery materials. Applying the WSP to the voltage profiles of A and B at the 0.1 C and 6 C discharge rate for a mass ratio of 1:1 wt% results in the voltage profiles depicted in Figure 5(a,b), respectively. As expected, both the voltage and the achieved capacity range between A and B. Figure 5(a,b) also shows the voltage profiles of the blended electrode obtained by ECM, which is basically a parallel connection of the components' behavior, instead of a superposition. In the case of 0.1 C, the

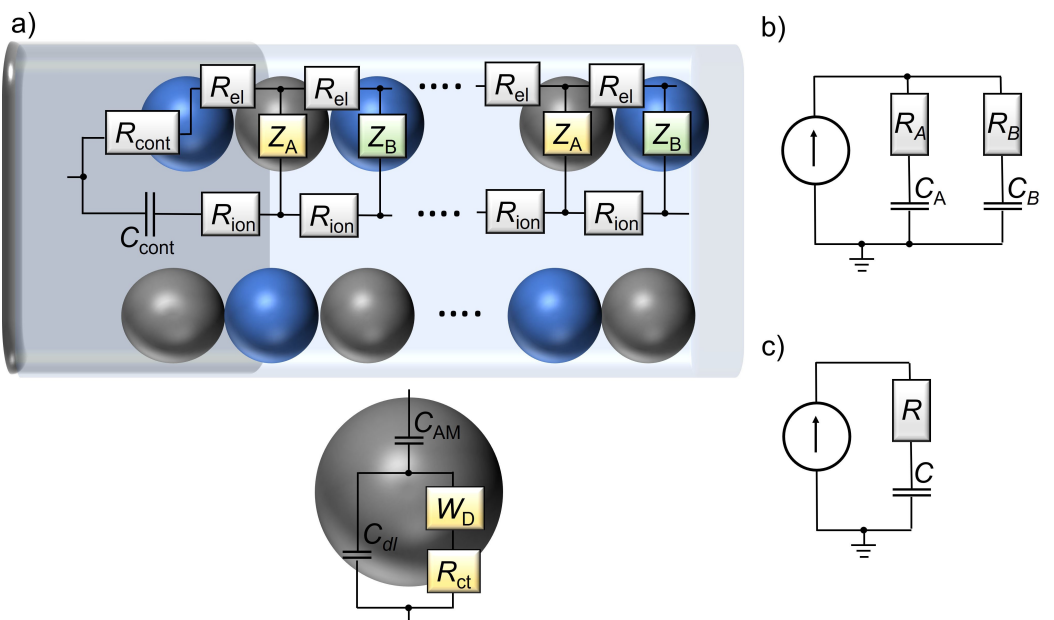


Figure 4. a) Schematic drawing of a porous insertion electrode with blended active materials, A and B, and equivalent circuit describing the electrochemical behavior of a blended Li-intercalation electrode. The Li-ion transport through the electrolyte and the electron conduction in the composite are described by a series of ohmic resistors, R_{el} and R_{ion} . The contact resistance between the porous composite and the current collector is modeled by an R - C -element, representing the interfacial resistance, R_{cont} , and the corresponding capacitance, C_{cont} . The inset shows details on the single particle level comprising the charge transfer resistance, R_{ct} , and the electrochemical double layer capacitance, C_{dl} . Solid-state diffusion in the active materials is represented by a Warburg element, W_D , and the Li-ion storage in the active material is modeled by the capacitance, C_{AM} . b, c) show simplified equivalent circuits to model the electrochemical behavior of b) blended and c) single component Li-intercalation electrodes with the resistors representing the sum of the individual resistors, which limit the Li insertion into components A and B.

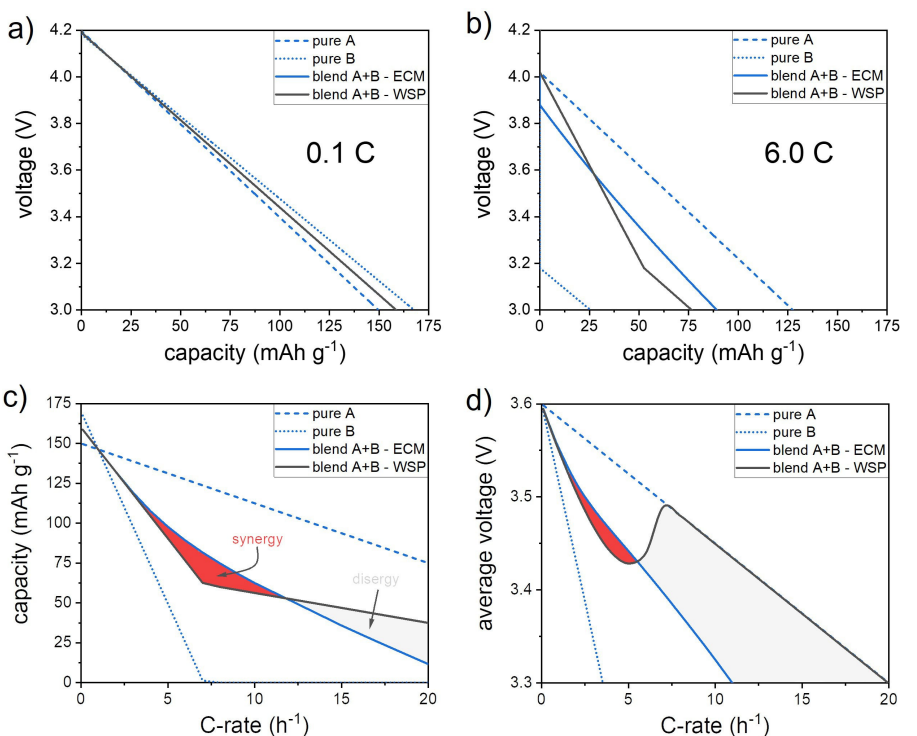


Figure 5. Voltage profiles of single component and blended electrodes at a) 0.1 C and b) 6 C. The voltage profiles of the blended electrodes were obtained by ECM or WSP. C-rate dependence of c) attained specific capacity and d) average voltage of single component and blended electrodes. Main differences between WSP and ECM results are associated with either synergy or disergy effects, indicated by the colored areas. Used parameters: $q_A = 150 \text{ mAh g}^{-1}$, $q_B = 170 \text{ mAh g}^{-1}$, $r_A = 0.2 \Omega \text{ g}$, $r_B = 1.0 \Omega \text{ g}$, A:B = 1:1 wt%. Details on the computations are provided as SI.

WSP and ECM approaches give similar voltage profiles. In contrast, for the 6 C discharge rate, the voltage profiles obtained by WSP and ECM show significant differences. Figure 5(c) shows the specific capacity for single material and blended electrodes obtained from WSP and ECM at different C-rates. At low discharge rates (< 3 C), both approaches give similar results for the blended electrodes. At medium to high discharge rates (3 C–12 C), ECM gives higher capacity when compared to the WSP. For very high discharge rates, the WSP gives significantly larger capacity than the ECM. Similarly, the average voltage is underestimated by the WSP in a specific range of C-rates and overestimated for high C-rates (Figure 5d). This behavior is in basic agreement with the experimental observations (cf. Figure 3c–f). Note again that the ECM performed here is not intended to simulate the experimental behavior of the LMO:LFP blend system, but is a simplified model for general understanding of specific aspects of blended electrodes. At medium to high discharge rates, the WSP underestimates the specific capacity and the average voltage, which corresponds to a synergistic effect according to the definition (b) given in the introduction.

To understand the origin of the differences between ECM and WSP predictions and thus the occurrence of synergy, we

analyzed the individual currents flowing through the components at different applied C-rates. Figure 6(a) shows the C-rates subjected to the components A and B in the blend at the nominal 0.1 C discharge rate for ECM and WSP. In both cases, the initial current is higher at A due to the lower resistance. In the course of discharging, the behavior predicted by ECM and WSP differs significantly. For the WSP, the entire current is consumed by A up to 0.2 ks. The supposed non-participation of B up to 0.2 ks results from the fact that the differential capacity of B is zero at the corresponding voltages due to the high resistance (Figure 6d). Only when a certain voltage is reached, B begins to contribute to the electrode reaction and the C-rates at A and B become identical. In contrast, considering the parallel connection of the components by ECM suggests that B contributes to the electrode reaction for the entire discharging process. In this case, the higher current at A results in a faster discharging of A and corresponding increase of the contribution of B. At a certain point, ECM predicts that the C-rates at A and B become identical and similar to the WSP prediction. In this case, the differences in the individual currents subjected to A and B hardly affect the corresponding capacities estimated from WSP and ECM (Figure 6g). However, the differences between WSP and ECM predictions increase with increasing C-

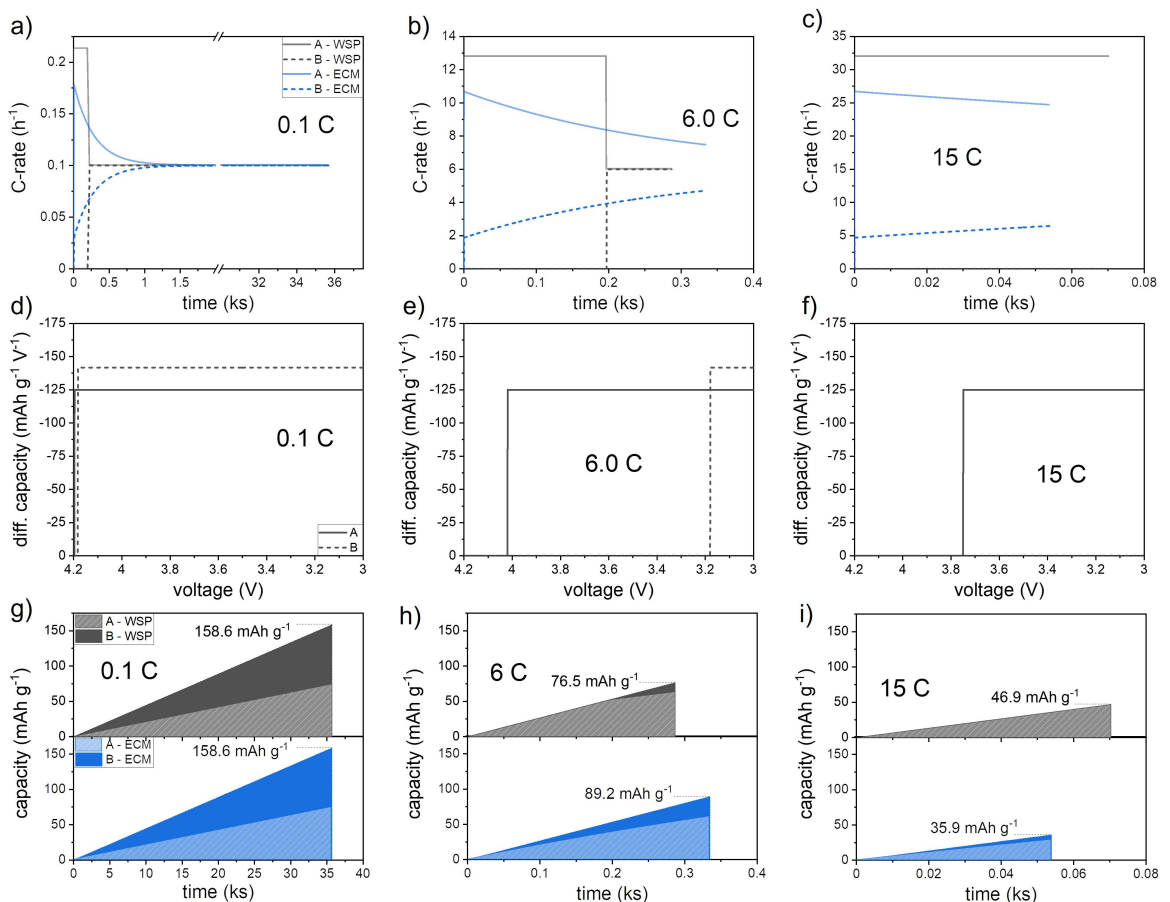


Figure 6. Comparative results obtained by WSP and ECM: Currents subjected to the component A (low resistance) and B (high resistance) in the blended electrode (1:1 wt%) at a) 0.1 C, b) 6 C and c) 15 C. Differential capacity used to determine voltage profiles by means of WSP at d) 0.1 C, e) 6 C and f) 15 C. Specific capacity development of the component A and B in the blended electrode at g) 0.1 C, h) 6 C and i) 15 C. Used parameters: $q_A = 150 \text{ mAh g}^{-1}$, $q_B = 170 \text{ mAh g}^{-1}$, $r_A = 0.2 \Omega \text{ g}$, $r_B = 1.0 \Omega \text{ g}$, A:B = 1:1 wt%. Details on the computations are provided as SI.

rate. At the 6 C discharge rate, the WSP predicts that the current at B is zero until approximately 0.2 ks (Figure 6b). In contrast, ECM predicts that B contributes to the electrode reaction for the entire discharging process, however, with an effective C-rate lower than the nominal one. This behavior is again caused by the differences in the resistances of A and B and results in significantly different contributions to the blend's capacity (Figure 6e). The WSP predicts slightly higher capacity contribution of A and much lower contribution of B when compared to the results obtained from ECM (Figure 6h). In total, this results in a lower capacity for the WSP approach compared to the results based on ECM. At very high rates, the WSP predicts that component B does not contribute to the electrode reaction anymore and the entire current is consumed by A (Figure 6c). Again, the ECM results show a different behavior with A and B contributing to the electrode reaction for the entire discharging process. In this case, the WSP predicts higher specific capacity of the blend due to the large contribution of A, overcompensating the losses of B (Figure 6i).

The percentage capacity utilization (Q/Q_{nominal}) of A and B in the blend predicted by WSP and ECM are shown in Figure 7. At low C-rates, the utilization of A and B agree for WSP and ECM. For medium to high C-rates, the utilization of the high-resistance component B is underestimated by the WSP, whereas the contribution of the low-resistance component A is overestimated. For a certain range of C-rates, this behavior results in an overestimation of the blend's capacity, marked in Figure 7 as "synergy region", that coincides with the behavior observed in Figure 5(c).

The observations in Figures 6 and 7 shed light on the origin of synergistic effects in blended electrodes. If the resistances of the components differ noticeably, the current is distributed among the components in a way that the voltage losses

become minimal. Accordingly, the high-resistance component can contribute to the electrodes capacity at nominal loads that actually exceed its rate capability by carrying smaller currents, whereby the low-resistance component accommodates higher currents than the nominal one. Consequently, the capacity contribution of the high-resistance component is larger than expected, whereas the capacity contribution of the low-resistance component is reduced according to the higher effective current. For a certain range of C-rates, the sum of the components' capacities in the parallel connection is larger than expected from the weighted superposition of their rate performances. In this case, the additional, unexpected capacity contribution of the high resistance component overcompensates the capacity losses of the low-resistance component caused by the higher effective current (cf. Figure 7). This means that the occurrence of synergy simply results from the parallel connection of the components and is thus an intrinsic property of blended electrodes. The extent of the synergistic effects depends on the properties of the active materials employed, as described in detail below in the context of a systematic parameter study. However, it should not go unmentioned that at very high rates, blending different active materials can also lead to a decrease in specific capacity (disergy) as indicated by the experimental and ECM results (cf. Figures 3 and 5). In this case, the effective C-rate at the low low-resistance component becomes very high and the corresponding capacity losses are not compensated by the additional, not expected contribution of the high-resistance component (cf. Figure 6). These relations must be considered when designing blended electrodes depending on the desired application, as discussed in detail below. For example, automotive industry targets charging times of less than 15 min and corresponding charging rates of 4–5 C. Accordingly, blended electrodes should be designed to maximize synergistic effects in this range of C-rates.

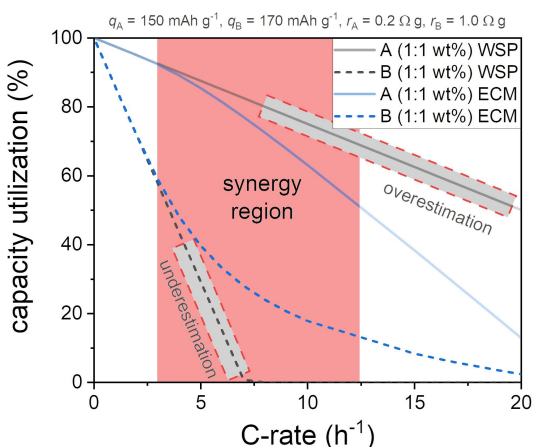


Figure 7. Comparison between the utilization (Q/Q_{nominal}) of component A (low resistance) and B (high resistance) in the blended (1:1 wt%) electrode determined by weighted superposition of the components' properties (WSP) and equivalent circuit modeling (ECM) for varying C-rate. Main differences in the specific capacity achieved are found for medium C-rates marked as "synergy region", where the additional contribution of B overcompensates losses of A, resulting in higher capacity than expected based on the weighted superposition of the components properties. Details on the computations are provided as SI.

2.3. Rational Design of Blended Electrodes

Generally, it is favorable to have active materials with both, high specific capacity and high rate capability. However, if an active material with favorable high capacity has low rate capability, the addition of a component with fast kinetics can improve overall performance beyond mere averaging, even if that component has a lower specific capacity than the base component. To identify the impact of the components' properties on the magnitude of synergistic effects, a straightforward parameter study has been performed. Figure 8 shows the magnitude of synergistic effects (capacity gain) by means of the percentage difference between WSP and ECM results for varying mass, resistance, and specific capacity ratios of the components. The magnitude and C-rate range of the capacity gain is largest for mass ratios around $\omega_A/\omega_B=1$ (Figure 8a) decreases more sharply as the proportion of the low-impedance component A increases compared to the high-impedance component B. As expected, Figure 8(b) shows that no synergy will occur if the components have similar specific resistance ($r_A/r_B \approx 1$). The larger the difference between r_A and

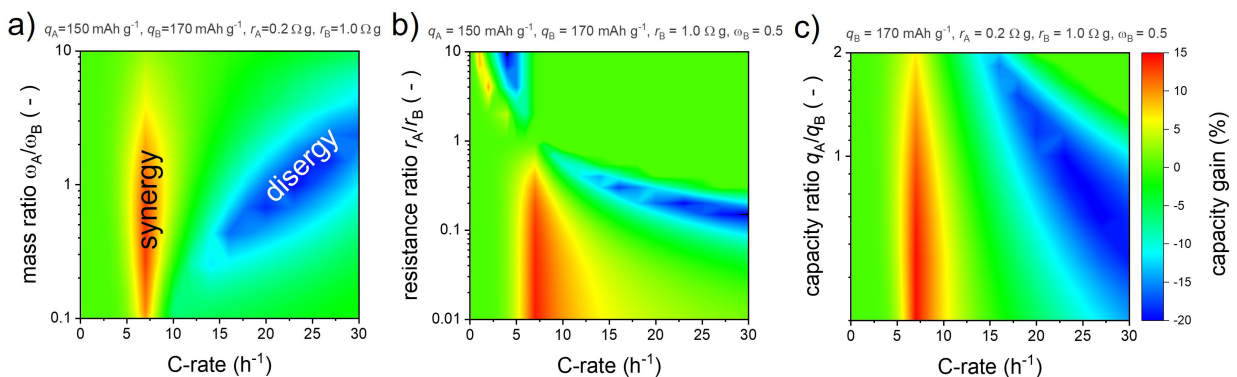


Figure 8. Magnitude of synergy/disergy effect by means of capacity compared between ECM and WSP results for varying a) mass ratio, b) resistance ratio, and c) specific capacity ratio of the components A and B depending on the C-rate. Positive (red) and negative (blue) values indicate synergy and disergy, respectively. Details on the computations are provided as SI.

r_B , the greater the magnitude of synergistic effects. Note that some quantitative aspects (e.g., the asymmetry between large values for r_A and r_B) are also related to the choice of the reference set of parameters, since the attainable capacity depends on the magnitude of the resistance, specific capacity of the components and their mass ratio. Figure 8(c) shows that magnitude and C-rate range of the capacity gain increases for decreasing specific capacity of the low resistance component A. These observations and dependencies agree with the own experimental results (Figure 3) and literature reports on synergistic effects in blended electrodes.^[15,17–22] In the present example of the LMO:LFP system, LFP has significantly higher resistance than LMO (cf. Figure S7). Accordingly, synergistic rate capability of LMO:LFP blended electrodes is found within a certain range of C-rates. The magnitude of the synergistic effect decreases with increasing mass fraction of low-resistant LMO (Figure 3), which is consistent with theoretical findings (Figure 8a and b). We want to point out that also aspects like the specific potential profiles of the components can have an impact on synergistic effects and might be considered in more detail by Multiphysics simulations. For reasons of clarity and in the sense of a conceptual clarification of the synergistic effects, simplified ECMs are used here. While certain quantitative aspects may differ for different systems, the qualitative statements, determined dependencies and conclusions remain valid.

Besides the rational design of blended electrodes in view of maximizing synergy effects arising from the parallel connection of the components, we want to emphasize that mixing several active materials can have further beneficial effects. Critical structural features of the porous composite electrode (e.g., tortuosity, interparticle contacts, or distribution of the carbon/binder domain), which determine the rate capability under diffusion limited conditions,^[4,33] can be influenced by blending. Particularly, it has already been shown that ionic and electronic percolation can be improved by targeted mixing of different active materials.^[20,34] These effects are mainly due to size, morphology and specific surface area of the particles employed, and the choice of binder and conductive additives as well as their processing during electrode fabrication, e.g., slurry preparation. Thus, the corresponding improvements are not

directly related to the nature of the active materials but result from concomitant microstructural and morphological factors. This makes it somewhat difficult to accurately predict the electrochemical behavior of blended electrodes based solely on the properties of the pure components. Therefore, electrochemical studies of blended electrodes should be considered together with imaging techniques to analyze 3D electrode structure and composition as well as modeling and simulation to account for internal dynamics. To this end, the findings on synergistic effects uncovered in this work are of crucial importance.

3. Conclusions

While empirical experience shows that mixing different active materials leads to improved electrode properties in Li-ion batteries, the underlying mechanisms have been poorly understood so far. Using straightforward equivalent circuit modeling combined with electrochemical studies, we illuminate the emergence of synergistic effects. It is found that the electrical parallel connection of the components in the composite electrodes allows the applied current to be distributed among the components in a way that the voltage losses become minimal. Consequently, a high-resistance component can contribute to the capacity of the blended electrode at loads that actually exceed its rate capability by carrying smaller currents, whereby the low-resistance component accommodates higher currents than the nominal one. For a certain range of C-rates, the sum of the components' capacities in the parallel connection is larger than expected from the weighted superposition of their rate performances. In this case, the additional, unexpected capacity contribution of the high resistance component overcompensates the capacity losses of the low-resistance component caused by the higher effective current. This means that the occurrence of synergy simply results from the parallel connection of the components and is thus an intrinsic property of blended electrodes. A comprehensive sensitivity analysis reveals that the extent of the synergistic effects depends on the properties of the active materials

employed. Particularly, the ratios of the individual rate capability, specific capacity and mass share of the components in the mixture affect the magnitude of synergistic effects in a complex manner. These relations must be considered when designing blended electrodes depending on the desired application. For example, automotive industry targets charging times of less than 15 min and corresponding charging rates of 4–5 C. Accordingly, blended electrodes should be designed to maximize synergistic effects in this range of C-rates. These findings greatly contribute to the understanding of the internal dynamics and synergy effects in blended electrodes and support the targeted development of advantageous material combinations and electrode designs for future Li-ion batteries.

Experimental Section

Electrode preparation

LiFePO₄ (LFP, Novarials) and LiMn₂O₄ (LMO, Novarials) powders and different active material mixtures were used for the electrode preparation with carbon black (Super P, Imerys) as conductive additive and polyvinylidene fluoride (PVDF 5130, Solvay) as binder. The slurries were mixed (0.5 h, 600 rpm) with the solvent N-Methyl-2-pyrrolidon (NMP 99.5%, VWR Chemicals) in a planetary ball mill (TMAX-DSP-LBPBM06A, Tmax Battery Equipments). The active material/conductive additive/binder ratio was 77/11.5/11.5 wt%. The slurries were coated (6 cm min^{-1} , 500 µm) on an Al-foil (15 µm, MTI Corp.) with an automatic film coater (JK-TMJ-20, Tmax Battery Equipments). Afterwards, the electrodes were dried under vacuum at 80 °C for at least 24 h. An overview of the materials and electrode properties is provided as SI (cf. Table S1).

Cell preparation

The electrodes were assembled under argon atmosphere (<1 ppm H₂O, <2 ppm O₂) using coin cells (CR2032, Hohsen). Sheets of metallic lithium (99.9%, Aldrich) were used as the counter electrodes and two layers of borosilicate-microfiber filter (CAT No. 5401-090 E, Whatman) functioned as the separator. 1 M LiPF₆ in a 1:1 wt% solution of ethylene carbonate and diethylene carbonate was applied as the electrolyte (150 µL).

Electrochemical characterization

The electrochemical measurements were performed in a climate test chamber (BIND9020-0199, Binder) using a potentiostat with integrated frequency response analyser (VMP3, Biologic). The cells were cycled several times (0.1 C) between 3 V and 4.2 V until stable conditions were reached ($\Delta q_{\text{discharge}} < 1\%$). Rate capability tests were conducted by charging the cells with a constant current (0.1 C) - constant voltage (4.2 V, 1 h) regime and subsequent discharging at different C-rates (0.1–10 C). Electrochemical impedance measurements were performed at open circuit potential with a p-p amplitude of 10 mV in a frequency range of 10^{-2} – 10^5 Hz.

Materials characterization

The electrodes were analyzed by scanning electron microscopy (NVision40, Zeiss). The cross-sectional preparation of the electrodes was performed using the broad ion preparation method (TIC020,

Leica). Phase analysis was carried out using a D8 Advance diffractometer (Bruker) with a Cu-K α X-ray tube and a 1D-detector.

Equivalent circuit modelling

Numerical computations of the voltage profiles have been done by implementing the fundamental equations that describe the equivalent circuits in MS Excel [Eqs. (S1–S17)]. To prove the correctness of the own calculations, the results were cross-checked using LTspice XVII software. Parameter studies were performed using a standard parameter set as the baseline (see Table S2). The equivalent circuit simulations were repeated varying a single parameter while all other parameters were fixed to the reference value.

Acknowledgements

The project this publication is based on was grant-aided by the German federal Ministry of Education and Research (BMBF) (grant no. 03XP0070B). The responsibility for the content of this publication is up to the authors. The electrodes and electrochemical cells were developed as part of the i-MIKE project supported by the European Union and the Free State of Saxony through the European Regional Development Fund (ERDF) (grant no. 100345909). Open Access funding enabled and organized by Projekt DEAL.

Conflict of Interest

The authors declare no conflict of interest.

Keywords: blended electrodes · kinetics · Li-ion batteries · rate performance · synergy

- [1] M. Armand, P. Axmann, D. Bresser, M. Copley, K. Edström, C. Ekberg, D. Guyomard, B. Lestriez, P. Novák, M. Petraníkova et al., *J. Power Sources* **2020**, 479, 22870.
- [2] Y. Ding, Z. P. Cano, A. Yu, J. Lu, Z. Chen, *Electrochim. Energy Rev.* **2019**, 2, 1.
- [3] R. Schmuck, R. Wagner, G. Hörpel, T. Placke, M. Winter, *Nat. Energy* **2018**, 3, 267.
- [4] C. Heubner, K. Nikłowski, S. Reuber, M. Schneider, M. Wolter, A. Michaelis, *Batteries & Supercaps* **2020**, 3, 1.
- [5] C. Heubner, S. Reuber, J. Seeba, P. Marcinkowski, K. Nikłowski, M. Schneider, M. Wolter, A. Michaelis, *J. Power Sources* **2020**, 479, 228704.
- [6] G. E. Blomgren, *J. Electrochim. Soc.* **2017**, 164, A5019.
- [7] Y. Huang, Y. Dong, S. Li, J. Lee, C. Wang, Z. Zhu, W. Xue, Y. Li, J. Li, *Adv. Energy Mater.* **2021**, 11, 2000997.
- [8] C. Heubner, T. Liebmann, M. Schneider, A. Michaelis, *Electrochim. Acta* **2018**, 269, 745.
- [9] S. B. Chikkannanavar, D. M. Bernardi, L. Liu, *J. Power Sources* **2014**, 248, 91.
- [10] M. Casas-Cabanas, A. Ponrouch, Palacín, M. Rosa, *Isr. J. Chem.* **2021**, 61, 26.
- [11] F. Dou, L. Shi, G. Chen, D. Zhang, *Electrochim. Energy Rev.* **2019**, 2, 149.
- [12] A. J. Smith, S. R. Smith, T. Byrne, J. C. Burns, J. R. Dahn, *J. Electrochim. Soc.* **2012**, 159, A1696.
- [13] T. Numata, C. Amemiya, T. Kumeuchi, M. Shirakata, M. Yonezawa, *J. Power Sources* **2001**, 97, 358.
- [14] J. Wang, Y. Yu, B. Li, P. Zhang, J. Huang, F. Wang, S. Zhao, C. Gan, J. Zhao, *ACS Appl. Mater. Interfaces* **2016**, 8, 20147.

- [15] G. Sun, S. Lai, X. Kong, Z. Chen, K. Li, R. Zhou, J. Wang, J. Zhao, *ACS Appl. Mater. Interfaces* **2018**, *10*, 16458.
- [16] K.-S. Lee, S.-T. Myung, D.-W. Kim, Y.-K. Sun, *J. Power Sources* **2011**, *196*, 6974.
- [17] J. F. Whitacre, K. Zaghib, W. C. West, B. V. Ratnakumar, *J. Power Sources* **2008**, *177*, 528.
- [18] K. G. Gallagher, S.-H. Kang, S. U. Park, S. Y. Han, *J. Power Sources* **2011**, *196*, 9702.
- [19] H. Cui, C. Yin, Y. Xia, C. Wei, W. Jiang, J. Sun, B. Qiu, M. Zhu, Z. Liu, *Ceram. Int.* **2019**, *45*, 15097.
- [20] N. M. Jobst, A. Hoffmann, A. Klein, S. Zink, M. Wohlfahrt-Mehrens, *ChemSusChem* **2020**, *13*, 3928.
- [21] A. Klein, P. Axmann, M. Wohlfahrt-Mehrens, *J. Electrochem. Soc.* **2016**, *163*, A1936.
- [22] A. Klein, P. Axmann, M. Wohlfahrt-Mehrens, *J. Power Sources* **2016**, *309*, 169.
- [23] K. Heo, J. Im, J.-S. Lee, J. Jo, S. Kim, J. Kim, J. Lim, *J. Electrochem. Sci. Technol.* **2020**, *11*, 282.
- [24] J.-S. Lee, K. Heo, H.-S. Kim, M.-Y. Kim, J. Kim, S.-W. Kang, J. Lim, *J. Alloys Compd.* **2019**, *781*, 553.
- [25] M. Qu, F. Nilsson, D. W. Schubert, *Nanotechnology* **2019**, *30*, 245703.
- [26] C. Heubner, T. Liebmann, C. Lämmel, M. Schneider, A. Michaelis, *J. Power Sources* **2017**, *363 C*, 311.
- [27] Z. Mao, M. Farkhondeh, M. Pritzker, M. Fowler, Z. Chen, *Electrochim. Acta* **2016**, *222*, 1741.
- [28] D. Wu, H. Ren, Y. Guo, X. Zhang, Z. Zhang, J. Li, *Ionics* **2018**, *265*, 174.
- [29] T. Liebmann, C. Heubner, M. Schneider, A. Michaelis, *Mater. Today Energy* **2021**, *22*, 100845.
- [30] Klaus J. Vetter, *Electrochemical Kinetics*, Elsevier, 1967.
- [31] A. Seaman, T.-S. Dao, J. McPhee, *J. Power Sources* **2014**, *256*, 410.
- [32] T. Schied, A. Nickol, C. Heubner, M. Schneider, A. Michaelis, M. Bobeth, G. Cuniberti, *ChemPhysChem* **2021**, *22*, 885.
- [33] C. Heubner, M. Schneider, A. Michaelis, *Adv. Energy Mater.* **2020**, *10*, 1902523.
- [34] N. Besnard, A. Etiemble, T. Douillard, O. Dubrunfaut, P. Tran-Van, L. Gautier, S. Franger, J.-C. Badot, E. Maire, B. Lestriez, *Adv. Energy Mater.* **2017**, *7*, 1602239.

Manuscript received: July 20, 2021

Revised manuscript received: October 15, 2021

Accepted manuscript online: October 18, 2021

Version of record online: November 8, 2021